ADVANCED ENERGY MATERIALS
www.advenergymat.de

Assembly-Free Fabrication of High-Performance Flexible Inorganic Thin-Film Thermoelectric Device Prepared by a Thermal Diffusion

Dong-Wei Ao, Wei-Di Liu, Zhuang-Hao Zheng, Xiao-Lei Shi, Meng Wei, Yi-Ming Zhong, Meng Li, Guang-Xing Liang, Ping Fan, and Zhi-Gang Chen**

High relative contact electrical resistance and poor flexibility in inorganic thin-film thermoelectric devices significantly limit their practical applications. To overcome this challenge, a one-step thermal diffusion method to fabricate assembly-free inorganic thin-film thermoelectric devices is developed, where the in situ grown electrode delivers an excellent leg-electrode contact, leading to high output power and flexibility in the prepared p-type Sb_2Te_3/n-type Bi_2Te_3 thin-film device, which is composed of 8 pairs of p-n junctions. Such a device shows a very low relative contact electrical resistance of 7.5% and a high power density of 1.42 mW cm^{-2} under a temperature difference of 60 K. Less than 10% change of the whole electrical resistance before and after bending test indicates the robust bending resistance and stability of the device. This study indicates that the novel assembly-free one-step thermal diffusion method can effectively enhance the leg-electrode contact, the device thermoelectric performance, bending resistance, and stability, which can inspire the development of thin-film thermoelectric devices.

1. Introduction

With the increasing demand for wearable power supplies on the internet of things,[1–4] flexible thin-film thermoelectric devices (TEDs) with unique advantages of wearability and scalability have attracted ever-increasing attention.[5–7] Typically, flexible thin-film TEDs are composed of highly flexible organic materials, such as polystyrene sulfonate acid (PEDOTS : PSS),[8] poly vinylidene fluoride,[9] polyaniline.[10] These devices exhibit high flexibility, where the key challenge lies in the low material performance. The overall material performance is evaluated by the dimensionless figure of merit, $ZT = S^2\sigma T/\kappa = S^2\sigma T/(\kappa_l + \kappa_e)$, and S, σ, T, κ, κ_l, and κ_e are the Seebeck coefficient, the electrical conductivity, the absolute temperature, the total thermal conductivity, the lattice thermal conductivity, and electrical thermal conductivities, respectively.[11–13] $S^2\sigma$ is generally defined as the power factor to estimate the overall electrical performance.[14] For typical p-type organic thermoelectric thin films, such as PEDOT:PSS, a room-temperature $S^2\sigma$ is generally <3 μW cm^{-1} K^{-2} with a corresponding $ZT < 0.3$.[15] For typical n-type organic thermoelectric thin films, such as PEDOT:PSS /CNTs, a room temperature ZT is generally <0.6.[16]

To overcome the low performance of organic flexible thin-film TEDs, high-performance inorganic thermoelectric thin-films are increasingly studied. Specifically, both n-type and p-type Bi_2Te_3-based thin-films have been reported with room-temperature ZT of ≈1.22 and ≈1.5, respectively.[17,18] HgSe-based thin-films have also been reported with a room-temperature ZT of ≈0.68.[19] Rongione et al.[20] further reported the room-temperature ZT value as high as ≈1.17 of SnSe-based thin-films. Additionally, high room-temperature $S^2\sigma$ as high as 25 μW cm^{-1} K^{-2} have also been reported in carbon nanotubes.[21] With such high materials performance, these inorganic thin-film thermoelectric materials have been assembled into flexible TEDs. For example, Kim et al.[1,22] prepared a flexible inorganic thin-film TED, which is composed of 72 pairs of p-type $Bi_{0.5}Sb_{1.5}Te_3$ and n-type $Bi_{0.5}Te_{2.7}Se_{0.3}$ legs and realized a high voltage output (V_{out}) of 693 mV under a temperature difference of 25.6 K. Yang et al.[3] reported a high output power (P_{out}) of 137.5 μW under a temperature difference of 19 K in

D.-W. Ao, Z.-H. Zheng, M. Wei, Y.-M. Zhong, G.-X. Liang, P. Fan
Shenzhen Key Laboratory of Advanced Thin Films and Applications
Key Laboratory of Optoelectronic Devices and Systems of Ministry of Education and Guangdong Province
College of Physics and Optoelectronic Engineering
Shenzhen University
Shenzhen 518060, P. R. China
E-mail: zhengzh@szu.edu.cn

W.-D. Liu
Australian Institute for Bioengineering and Nanotechnology
The University of Queensland
Brisbane, Queensland 4072, Australia

X.-L. Shi, M. Li, Z.-G. Chen
School of Chemistry and Physics
Queensland University of Technology
Brisbane, Queensland 4001, Australia
E-mail: zhigang.chen@qut.edu.au

The ORCID identification number(s) for the author(s) of this article can be found under https://doi.org/10.1002/aenm.202202731.

DOI: 10.1002/aenm.202202731

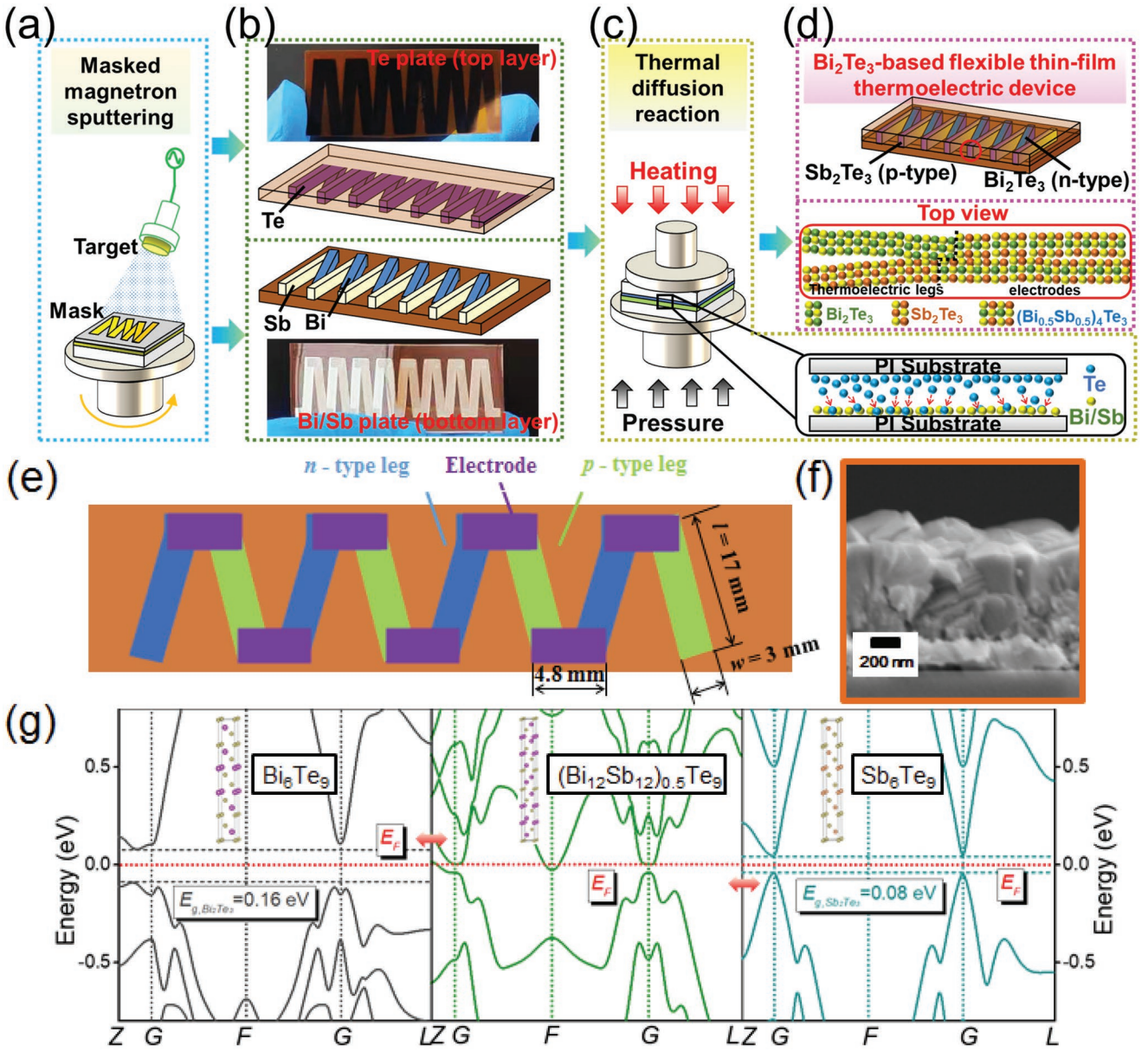

Figure 1. Schematic diagrams of the preparation of Bi_2Te_3-Sb_2Te_3 flexible thin-film: a) masked magnetron sputtering process to prepare b) as-designed precursor thin-film plates, including the Te plate and the Bi/Sb plate; c) thermal diffusion raction prcoess for Bi_2Te_3-Sb_2Te_3 thin-film device preparation and d) as-grown Bi_2Te_3-Sb_2Te_3 thin-film device with a schematic material structure at the joint point between p-type Sb_2Te_3 and n-type Bi_2Te_3 legs. e) The diagram schematic of the devices. f) The morphology of the electrode across the vertical section. g) Calculated electronic band structures of n-type Bi_6Te_9, p-type Sb_6Te_9, and $(Bi_{12}Sb_{12})_{0.5}Te_9$ with corresponding crystal structures.

stretchable Bi_2Te_3-based flexible thin-film TEDs. However, these devices present relative low P_{out} of <1.0 mW under a temperature difference of 47.5 K[23] comparing with the bulk counterparts (≈0.93 W[24]). One main reason for this relatively lower P_{out} is the high relative contact electrical resistance ($R_{cont}/R_{in,exp}$, R_{cont} is the contact electrical resistance and $R_{in,exp}$ is measured internal electrical resistance) because of the poor contact between the thermoelectric legs and electrodes. Yamamuro et al.[25] also prepared a flexible n-type Bi_2Te_3 and p-type Sb_2Te_3 thin-film TED with the R_{cont} as high as ≈3.4 kΩ, which is ≈30% of the R_{total}. Eom et al.[26] also reported the high $R_{cont}/R_{in,exp}$ of the flexible thin-film TED of ≈15%. The poor leg/electrode contact and high $R_{cont}/R_{in,exp}$ can intervene the carrier transport and correspondingly deteriorate the P_{out} of TED,[27,28] which severely limits the P_{out} of flexible thin-film TEDs.

To overcome this challenge, we innovatively employ a one-step thermal diffusion method for the assembly-free fabrication of a Bi_2Te_3-Sb_2Te_3 thin-film device, as shown in **Figure 1**. Firstly, a top tellurium plate and a bottom Sb/Bi plate are prepared by using a masked magnetron sputtering method (Figure 1a,b), and then stacked together under external heating and pressure (Figure 1c), aiming to boost the diffusion of Te and the formation of Bi_2Te_3-Sb_2Te_3 flexible thin-film TED in one step. In the subsequent thermal diffusion reaction process, the electrode materials form together with the Bi_2Te_3 and Sb_2Te_3 thermoelectric legs as shown in Figure 1d. The in situ grown

electrodes secure good contact bewteen the electrodes and thermoelectric legs and achieve low $R_{cont}/R_{in,exp}$. As can be seen, Fermi level (E_F) of the $(Bi_{0.5}Sb_{0.5})_4Te_3$ electrode lies in the conduction band indicating metallic behavior and high σ of this material. Meanwhile, Bi_2Te_3 and Sb_2Te_3 have shown n-type and p-type semiconducting behaviors as the E_F locates at the band gap close to the conduction band and valence band, respectively. Correspondingly, while the E_F of different materials is aligned, the metallic $Bi_2Sb_2Te_3$ electrodes can effectively facilitate the carrier transport. Thus, density funtional theory calculation indicates the metal $Bi_2Sb_2Te_3$ electrodes effectively facilitate the carrier transport within the p-n junctions (Figure 1f). Our experimental results demonstrate that the in situ grown $(Bi_{0.5}Sb_{0.5})_4Te_3$ electrodes can approach a low $R_{cont}/R_{in,exp}$ of 7.5%, leading to a high power density (ω_{max}) of 1.42 mW cm^{-2} at a temperature difference (ΔT) of ≈60 K in the as-fabricated TED that is composed of only 8 pairs of thermoelectric legs. During the >2000 bending cycles the relative electrical resistance ($\Delta R/R_0$, ΔR is the electrical resistance changing with bending cycles and R_0 is the initial electrical resistance before bending) is ranging from 100% to 110%, indicating the robust flexibility and stability of the as-fabricated TED.

2. Results and Discussion

Figure 2a shows a photograph of the Bi_2Te_3-Sb_2Te_3 flexible thin-film, prepared by the thermal diffusion method. XRD, SEM-EDS and TEM analyses are employed to investigate the structural information of the p-type Sb_2Te_3 leg, n-type Bi_2Te_3 leg and the joint electrodes. Figure 2b shows the material characterization results of the p-type Sb_2Te_3 leg. The XRD pattern (Figure 2b1) reveals that only Sb_2Te_3 phase (JCPDS 15-0874) is existed and only Sb and Te are observed in the SEM-EDS maps (Figure 2b2). Corresponding HRTEM image clearly shows the lattice can well superimpose with the crystal structure of Sb_2Te_3 and further confirmed the high crystallinity. Figure 2c shows the material characterization results of the n-type Bi_2Te_3 leg, where the legs are also composed of highly crystallized Bi_2Te_3 (JCPDS 15-0863) without other obvious impurities. Figure 2d shows the XRD pattern of the joint electrode area, which shows that they are composed of $(Bi_{0.5}Sb_{0.5})_4Te_3$ (JCPDS 72-1838) without obvious impurities.

To understand the bending resistance and stability of as-assembled Bi_2Te_3-Sb_2Te_3 thin-film TED, we conducted bending test on the Bi_2Te_3 film, Sb_2Te_3 film, and Bi_2Te_3-Sb_2Te_3 TED as shown in **Figure 3**. And the initial resistances of as-prepared Bi_2Te_3 and Sb_2Te_3 thin films are ≈225 and ≈75 Ω (the bending information as present in Supporting Information). Figure 3a,b show the bent and unbent statuses of the Bi_2Te_3 and Sb_2Te_3 thin-films during the bending test. Figure 3c,d show the $\Delta R/R_0$ of the Bi_2Te_3 and Sb_2Te_3 thin-films as a function of bending cycles and radius. The $\Delta R/R_0$ values of both Bi_2Te_3 and Sb_2Te_3 films are <110% even after 2000 bending cycles under a small bending radius of 8 mm. When the bending radius is as small as 6.5 mm, the $\Delta R/R_0$ value are also <110%. The small change of $\Delta R/R_0$ as a function of both bending cycles and radius demonstrates high bending resistance and stability of as-prepared

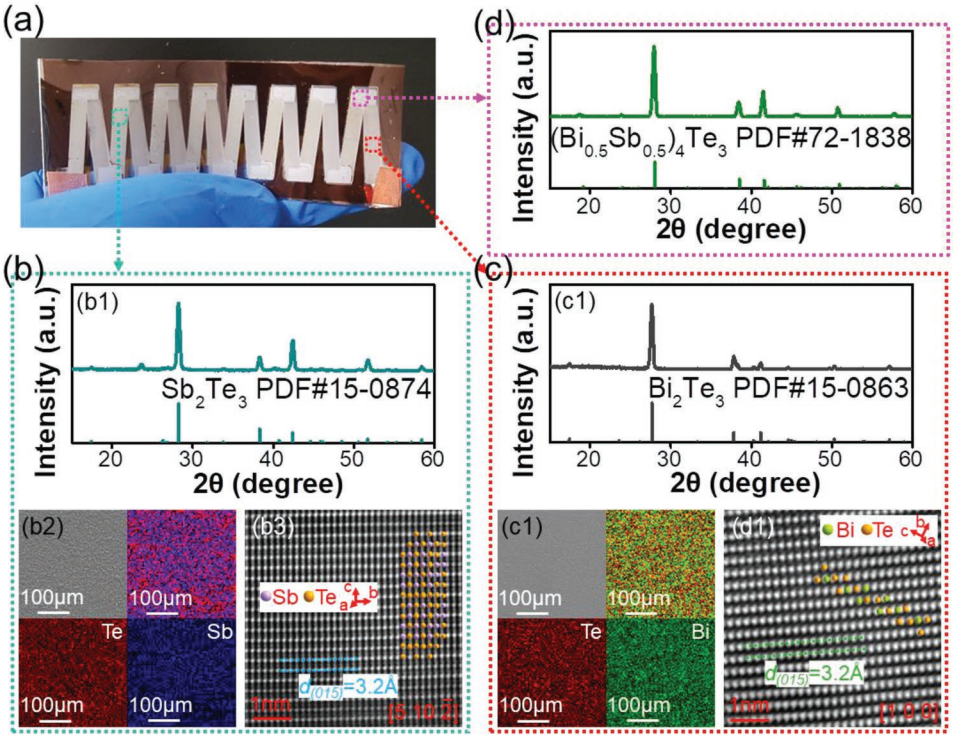

Figure 2. a) Photograph of as-prepared Bi_2Te_3-Sb_2Te_3 thin-film device and corresponding characterizations of b) p-type Sb_2Te_3-legs, c) n-type Bi_2Te_3-legs, and d) the joint point between p-type Sb_2Te_3 and n-type Bi_2Te_3 legs, where (b1), (c1), and (d) are the XRD patterns, (b2) and (c2) are the SEM-BSE images and corresponding EDS maps, (b3) and (c3) are the HRTEM images.

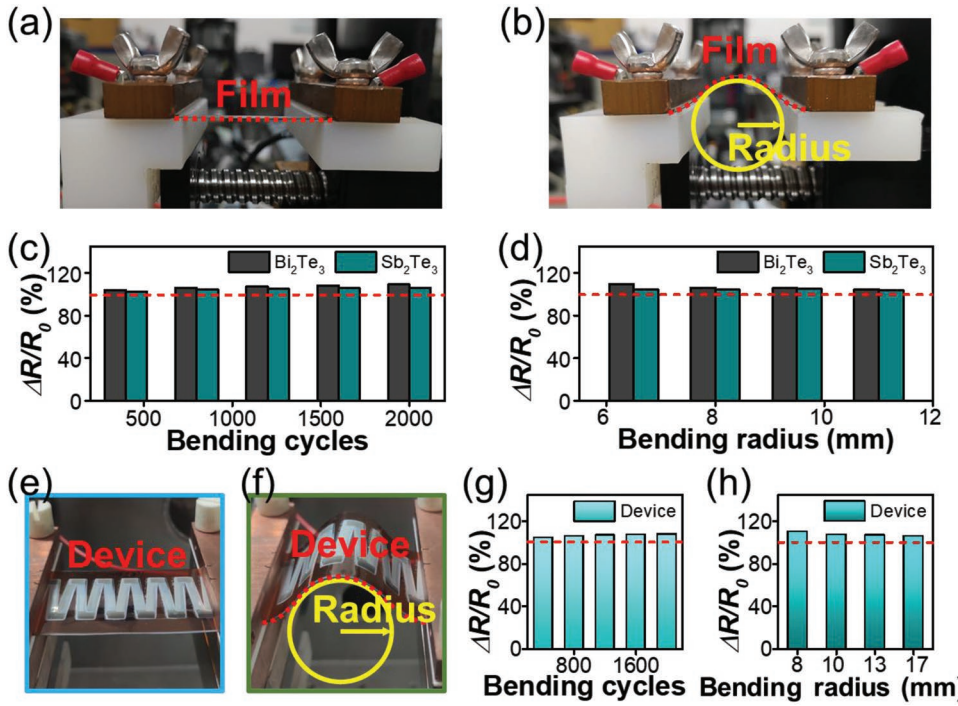

Figure 3. Photograph of the Bi_2Te_3 and Sb_2Te_3 film bending test process, where a) is a flat film and b) is a bent film on the bending platform, respectively. Film bending test results, where c) is the $\Delta R/R_0$ as a function of bending cycles under the bending radius of 8 mm, and d) is the $\Delta R/R_0$ as a function of bending radius under the bending cycles of 800. Photograph of the Bi_2Te_3-Sb_2Te_3 thin-film device bending test process, where e) is the flat device and f) is the bent device on the bending platform, respectively. Device bending test results, where g) is the $\Delta R/R_0$ as a function of bending cycles under the bending radius of 17 mm, and h) is the $\Delta R/R_0$ as a function of bending radius under the bending cycles of 800.

Bi_2Te_3 and Sb_2Te_3 thin-films. Figure 3e,f present the bent and unbent statuses of the Bi_2Te_3-Sb_2Te_3 thin-film device. It should be noted that the samples in looks different in Figure 3e,f should be attributed to the change of environment light as the photographs are taken at different time. And Figure 3g,h show the $\Delta R/R_0$ as a function of the bending cycles and bending radius. Due to the well connection between the thermoelectric legs and the electrodes, the as-prepared Bi_2Te_3-Sb_2Te_3 thin-film device also shows high bending resistance and stability as evidenced by the <110% change of $\Delta R/R_0$ after 2000 bending cycles and under different bending radiuses.

To evaluate the thermoelectric performance of the Bi_2Te_3-Sb_2Te_3 thin-film TED, we firstly measured the thermoelectric performance of as-prepared Bi_2Te_3 and Sb_2Te_3 thin-films as shown in **Figure 4**a–c. Figure 4a plots the measured temperature-dependent σ of the Bi_2Te_3 and Sb_2Te_3 thin-films. Within the device test temperature range (from 297 to 357 K), the average σ of the Bi_2Te_3 and Sb_2Te_3 thin-films is 528 and 1452 S cm^{-1}. The corresponding average |S| of the Bi_2Te_3 and Sb_2Te_3 thin-films is 165 and 105 μV K^{-1}, as shown in Figure 4b. Figure 4c shows the carrier concentration (n_H for p-type Sb_2Te_3 and n_e for n-type Bi_2Te_3)-dependent room-temperature $S^2\sigma$ of as-prepared p-type Sb_2Te_3 and n-type Bi_2Te_3 thin-films in comparison with the SPB model calculated values. The calculation process of the SPB model is shown in Equations (S1)–(S5) (Supporting Information). As can be seen, with the n_H or n_e close to the optimal level (≈1×10^{19} cm^{-3}). The room-temperature $S^2\sigma$ of the p-type Sb_2Te_3 and n-type Bi_2Te_3 has approached 16.59 and 14.58 μW cm^{-1} K^{-2}, respectively, which are close to the maximum values and demonstrate high thermoelectric performance.

To evaluate the overall thermoelectric performance of as-prepared Bi_2Te_3-Sb_2Te_3 thin-film TED, we further measured the device performance, as shown in Figure 4d–h. Figure 4d shows the internal resistance (R_{in}) by comparing the theoretical values ($R_{in,theor}$) of the Bi_2Te_3-Sb_2Te_3 thin-film TED with the $R_{in,exp}$ of three repeatedly prepared Bi_2Te_3-Sb_2Te_3 thin-film TEDs. As can be seen, the $R_{in,exp}$ values of as-prepared Bi_2Te_3-Sb_2Te_3 thin-film TEDs are closely consistent of ≈2398 Ω, which is slightly higher than the $R_{in,theor}$ (2230 Ω) due to additional contact electrical resistance (R_{cont}). Figure 4e shows the open-circuit voltage (V_{oc}) by comparing the measured values ($V_{oc,exp}$) with the theoretical values ($V_{oc,theor}$) when the temperature difference (ΔT) ranges from 10 to 60 K under the cold-site temperature (T_{cold}) of 300 K. As can be seen, the V_{oc} increases significantly with increasing the temperature difference and the $V_{oc,exp}$ is slightly higher than the $V_{oc,theor}$, which is possibly due to non-linear temperature gradient.[29] With increasing the temperature difference to as high as 60 K, the $V_{oc,exp}$ approaches as high as 140 mV. Figure 4f plots the $R_{cont}/R_{in,exp}$ of the Bi_2Te_3-Sb_2Te_3 thin-film TED in this study with others.[25,26,30–39] As can be seen, our relative contact electrical resistance (the calculation process as presented in Supporting Information) is only at ≈7.5%, indicating that our in situ electrode growth can significantly enhance the contact between the thermoeletric legs and electrodes. The inset of Figure 4f shows a photograph, which displays the application of as-prepared Bi_2Te_3-Sb_2Te_3 thin-film TED

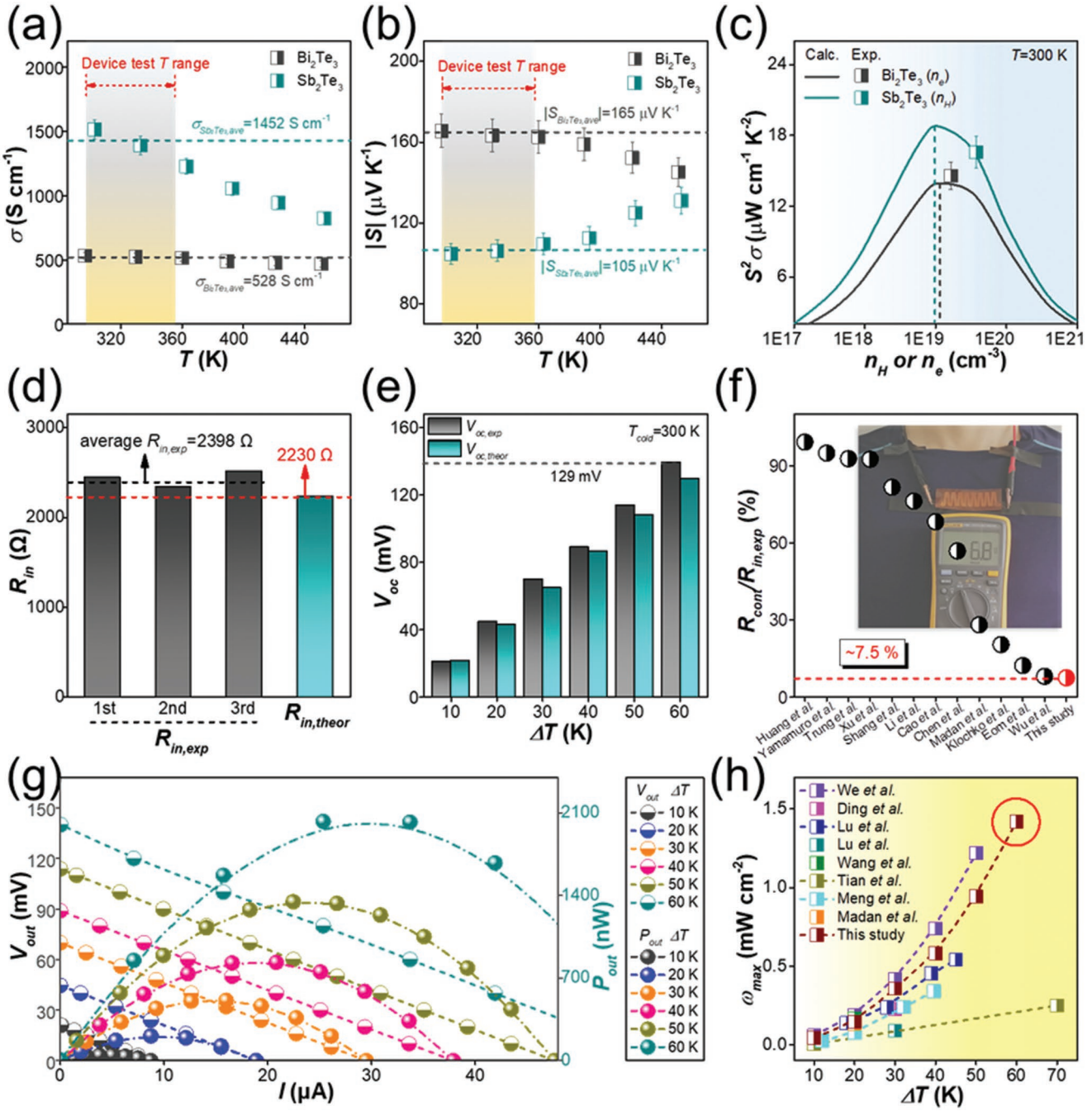

Figure 4. Measured thermoelectric performance of as-prepared Bi_2Te_3 and Sb_2Te_3 thin-films, where a) is the σ as a function of temperture, b) is the $|S|$ as a function of temperature, and c) is the room-temperature $S^2\sigma$ as a function of n_H (for p-type Sb_2Te_3) or n_e (for n-type Bi_2Te_3). d) Repeatedly measured room-temperature R_{in} of as-prepared Bi_2Te_3-Sb_2Te_3 flexible device in comparison with the theoretical value. e) Measured V_{oc} 140 mV of as-prepared Bi_2Te_3-Sb_2Te_3 flexible device in comparison with the theoretical values under different hot-cold side temperature differences, where the cold-side temperature is 300 K. f) Comparison between the $R_{cont}/R_{in,exp}$ of as-prepared Bi_2Te_3-Sb_2Te_3 thin-film device in this study with others,[25,26,30–39] and inset is the photograph of applying as-prepared Bi_2Te_3-Sb_2Te_3 thin-film device for wearable power generating. g) Measured V_{out} and P_{out} of as-prepared Bi_2Te_3-Sb_2Te_3 thin-film device as a function of I under different hot-colde side temperature differences. h) Evaluated ω_{max} of as-prepared Bi_2Te_3-Sb_2Te_3 thin-film device in comparison with other state-of-art flexbiel thin-film TEDs.[15,37,40–45]

for wearable power generation utilizing the temperature difference between human body and the ambient environment. When used as wearable power generator, the maximum V_{oc} is 6.8 mV under a temperature difference of ≈5 K. Figure 4g presents the V_{out} and the P_{out} of the Bi_2Te_3-Sb_2Te_3 thin-film TED as a function of current (I) under various temperature difference. With increasing the temperature difference, the maximum P_{out} and corresponding V_{out} and I increase. Here, the maximum P_{out} can approach as high as ≈2000 nW under the temperature difference of 60 K. Figure 4h shows corresponding maximum ω_{max}, which approaches as high

as 1.420 mW cm^{-2} under the temperature difference of 60 K, which is higher than other state-of-art thin-film-based flexible TEDs, including Bi_2Te_3,[37] Bi_2Te_3/Sb_2Te_3,[15] Ag_2Se,[40] Ag_2Se/Ag/CuAgSe,[41] PEDOT:PSS/Cu_2Se,[42] C60/TiS_2,[43] TiS_2/organic-[44] and Polyvinylpyrrolidone/Ag/Ag_2Te[45]-based TEDs.

3. Conclusion

In summary, we have successfully prepared an entire flexible Bi_2Te_3-Sb_2Te_3 thin-film-based TED on polyimide substrates by using an assembly-free one-step thermal diffusion process. During this process, the in situ grown electrode together with the highly crystallized Sb_2Te_3 and Bi_2Te_3 thermoelectric legs secures good contact between the electrodes and the thermoelectric legs in the as-fabricated TED, composed of 8 pairs of p-n junctions. The as-fabricated TED shows a very low R_{cont} of ≈7.5% of the $R_{in,exp}$, high V_{oc} of ≈129 mV, and high ω_{max} of 1.42 mW cm^{-2} under a ΔT of 60 K. Our study indicates that thermal diffusion method can contribute to ultralow $R_{cont}/R_{in,exp}$ and boost the development of highly flexible high-performance fully inorganic Bi_2Te_3-Sb_2Te_3 thin-film-based TEDs.

Supporting Information

Supporting Information is available from the Wiley Online Library or from the author.

Acknowledgements

D.W.A., W.D.L., and Z.H.Z. contributed equally to this work. This work was supported by the National Natural Science Foundation of China (Grant No. 11604212), the National Natural Science Foundation of Guangdong province of China (2020A1515010515 and 2022A1515010929), Science and Technology plan project of Shenzhen (20200811230408001). Z.G.C. thanks the financial support from Australia Research Council, Innovation Centre for Sustainable Steel Project and QUT capacity building professor program. The authors are thankful for the assistance on STEM-HAADF observation received from the Electron Microscope Center of the Shenzhen University. For all human body-related experiments with wearable sensors, informed written consent was obtained from all participants prior to data collection for the research.

Open access publishing facilitated by Queensland University of Technology, as part of the Wiley - Queensland University of Technology agreement via the Council of Australian University Librarians.

Conflict of Interest

The authors declare no conflict of interest.

Data Availability Statement

The data that support the findings of this study are available from the corresponding author upon reasonable request.

Keywords

flexible devices, thermal diffusion, thermoelectric legs, thin-films

Received: August 10, 2022
Published online: September 14, 2022

[1] X. L. Shi, J. Zou, Z. G. Chen, *Chem. Rev.* **2020**, *120*, 7399.
[2] B. Jabar, X. Y. Qin, A. Mansoor, H. W. Ming, L. L. Huang, M. H. Danish, J. Zhang, D. Li, C. Zhu, H. X. Xin, C. J. Song, *Nano Energy* **2021**, *80*, 105512.
[3] Y. Yang, H. Hu, Z. Chen, Z. Wang, L. Jiang, G. Lu, X. Li, R. Chen, J. Jin, H. Kang, H. Chen, S. Lin, S. Xiao, H. Zhao, R. Xiong, J. Shi, Q. Zhou, S. Xu, Y. Chen, *Nano Lett.* **2020**, *20*, 4445.
[4] W. D. Liu, L. Yang, Z. G. Chen, *Nano Today* **2020**, *35*, 100938.
[5] Q. Zhou, K. Zhu, J. Li, Q. Li, B. Deng, P. Zhang, Q. Wang, C. Guo, W. Wang, W. S. Liu, *Adv. Sci.* **2021**, *8*, 2004947.
[6] Y. Wang, Y. Lei, X. L. Shi, S. Xun, L. D. Liu, M. S. Dargusch, J. Zou, Z. G. Chen, *Adv. Mater.* **2019**, *31*, 1807916.
[7] S. Y. He, Y. B. Li, L. Liu, Y. Jiang, J. J. Feng, W. Zhu, J. Zhang, Z. Dong, Y. Deng, J. Luo, W. Zhang, G. Chen, *Sci. Adv.* **2020**, *6*, 8423.
[8] Y. Wang, M. Hong, W. D. Liu, X. L. Shi, S. Xu, Q. Sun, H. Gao, S. Lu, J. Zou, Z. G. Chen, *Chem. Eng. J.* **2020**, *397*, 125360.
[9] Y. Xue, Z. Zhang, Y. Zhang, X. Wang, L. Li, H. Wang, G. Chen, *Carbon* **2020**, *157*, 324.
[10] Y. Wang, S. Zhang, M. Y. Deng, *J. Mater. Chem. A* **2016**, *4*, 3554.
[11] S. D. Xu, X. L. Shi, M. Dargusch, ChonganD. , JinZ. , Z. G. Chen, *Prog. Mater. Sci.* **2021**, *121*, 100840.
[12] X. L. Shi, W. Y. Chen, T. Zhang, J. Zou, Z. G. Chen, *Energy Environ. Sci.* **2021**, *14*, 729.
[13] W. D. Liu, Y. Yu, M. Dargusch, Q. F. Liu, Z. G. Chen, *Renewable Sustainable Energy Rev.* **2021**, *141*, 110800.
[14] W. D. Liu, D. Z. Wang, Q. F. Liu, W. Zhou, Z. P. Shao, Z. G. Chen, *Adv. Energy Mater.* **2020**, *10*, 2000367.
[15] J. H. We, S. J. Kim, B. J. Cho, *Energy* **2014**, *73*, 506.
[16] H. Wang, J. H. Hsu, S. I. Yi, S. L. Kim, K. Choi, G. Yang, C. Yu, *Adv. Mater.* **2015**, *27*, 6855.
[17] D. L. Qin, F. Pan, J. Zhou, Z. Xu, Y. Deng, *Nano Energy* **2021**, *89*, 106472.
[18] M. Tan, W. D. Liu, X. L. Shi, J. Shang, H. Li, X. B. Liu, L. Z. Kou, M. Dargusch, Y. Deng, Z. G. Chen, *Nano Energy* **2019**, *78*, 105379.
[19] J. Choi, K. Cho, J. Yun, Y. Park, S. Yang, S. Kim, *Adv. Energy Mater.* **2017**, *7*, 1700972.
[20] N. A. Rongione, M. Li, H. Wu, H. D. Nguyen, J. S. Kang, B. Ouyang, H. Xia, Y. Hu, *Adv. Electron. Mater.* **2019**, *1800774*, 12819.
[21] C. J. An, Y. H. Kang, A. Y. Lee, K. S. Jang, Y. Jeong, S. Y. Cho, *ACS Appl. Mater. Interfaces* **2016**, *8*, 22142 .
[22] S. J. Kim, H. Choi, Y. Kim, J. H. We, J. S. Shin, H. E. Lee, M. W. Oh, K. J. Lee, B. J. Cho, *Nano Energy* **2017**, *31*, 258.
[23] Y. Y. Zheng, Q. Zhang, W. Jin, Y. Jing, X. Chen, X. Han, Q. Bao, Y. Liu, X. Wang, S. Wang, Y. Qiu, C. Di, K. Zhang, *J. Mater. Chem. A* **2020**, *6*, 2984.
[24] G. J. Snyder, J. R. Lim, C. K. Huang, J. P. Fleurial, *Nat. Mater.* **2003**, *2*, 528.
[25] H. Yamamuro, N. Hatsuta, M. Wachi, Y. Takei, M. Takashiri, *Coatings* **2018**, *8*, 22.
[26] Y. Eom, D. Wijethunge, H. Park, S. H. Park, W. Kim, *Appl. Energy* **2017**, *206*, 649.
[27] H. S. Kim, W. S. Liu, Z. F. Ren, *Energy Environ. Sci.* **2017**, *10*, 69.
[28] X. D. Zhu, L. L. Cao, W. Zhu, Y. Deng, *Adv. Mater. Interfaces* **2018**, *5*, 1801279.
[29] A. A. Melnikov, V. G. Kostishin, V. V. Alenkov, *J. Electron. Mater.* **2016**, *46*, 2737.
[30] X. L. Huang, D. W. Ao, T. B. Chen, Y. X. Chen, F. Li, S. Chen, G. X. Liang, X. H. Zhang, Z. H. Zheng, P. Fan, *Mater. Today Energy* **2021**, *21*, 100743.
[31] N. H. Trung, N. V. Toan, T. Ono, *Appl. Energy* **2018**, *210*, 467.
[32] Z. Xu, J. Li, X. Tang, Y. Liu, T. Jiang, Z. Yuan, K. Liu, *Energy* **2020**, *194*, 116873.
[33] H. J. Shang, T. G. Li, D. Luo, L. Yu, Q. Zou, D. X. Huang, L. Y. Xiao, H. W. Gu, Z. F. Ren, F. Z. Ding, *ACS Appl. Mater. Interfaces* **2020**, *12*, 7358.

[34] J. Li, X. Tang, Y. Liu, Z. Yuan, Z. Xu, K. Liu, *Energy Technol.* **2019**, *7*, 1800707.
[35] Z. Cao, M. J. Tudor, R. N. Torah, S. P. Beeby, *IEEE Trans. Electron Devices* **2016**, *63*, 4024.
[36] A. Chen, D. Madan, P. K. Wright, J. W. Evans, *J. Micromech. Microeng.* **2011**, *21*, 104006.
[37] D. Madan, Z. Q. Wang, A. Chen, R. C. Juang, J. Keist, P. K. Wright, J. W. Evans, *ACS Appl. Mater. Interfaces* **2012**, *4*, 6117.
[38] N. P. Klochko, V. A. Barbash, K. S. Klepikova, V. R. Kopach, I. I. Tyukhov, O. V. Yashchenko, D. O. Zhadan, S. I. Petrushenko, S. V. Dukarov, V. M. Lyubov, A. L. Khrypunova, *Sol. Energy* **2020**, *201*, 21.
[39] B. Wu, Y. Guo, C. Hou, Q. Zhang, Y. Li, H. Wang, *Adv. Funct. Mater.* **2019**, *29*, 1900304.
[40] Y. Ding, Y. Qiu, K. Cai, Q. Yao, S. Chen, L. Chen, J. He, *Nat. Commun.* **2019**, *10*, 841.
[41] Y. Lu, Y. Qiu, K. F. Cai, Y. F. Ding, M. D. Wang, C. Jiang, Q. Yao, C. Huang, L. D. Chen, J. Q. He, *Energy Environ. Sci.* **2020**, *13*, 1240.
[42] Y. Lu, F. Y. Ding, Y. Qiu, K. F. Cai, Q. Yao, H. J. Song, L. Tong, J. Q. He, L. D. Zhao, *ACS Adv. Mater. Interfaces* **2019**, *11*, 12819.
[43] L. M. Wang, Z. M. Zhang, L. X. Geng, T. Yuan, Y. Liu, J. Guo, L. Fang, J. Qiu, S. Wang, *Energy Environ. Sci.* **2018**, *11*, 1307.
[44] R. M. Tian, C. Wan, Y. Wang, Q. Wei, T. Ishida, A. Yamamoto, A. Tsuruta, W. Shin, S. Li, K. Koumoto, *J. Mater. Chem. A* **2017**, *5*, 56294.
[45] Q. Meng, Y. Qiu, K. Cai, Y. Ding, M. Wang, H. Pu, Q. Yao, L. Chen, J. He, *ACS Appl. Mater. Interfaces* **2019**, *11*, 33254.